NANO LETTERS
Letter
Cite This: Nano Lett. 2018, 18, 7816−7821
pubs.acs.org/NanoLett

Asymmetric Ionic Conditions Generate Large Membrane Curvatures

Marzieh Karimi,[†] Jan Steinkühler,[†] Debjit Roy,[†,§] Raktim Dasgupta,[†,‡] Reinhard Lipowsky,[†] and Rumiana Dimova*[,†]

[†]Department of Theory and Bio-Systems, Max Planck Institute of Colloids and Interfaces, Science Park Golm, 14424 Potsdam, Germany

[‡]Laser Biomedical Applications Section, Raja Ramanna Centre for Advanced Technology, 452013 Indore, India

Supporting Information

ABSTRACT: Biological membranes possess intrinsic asymmetry. This asymmetry is associated not only with leaflet composition in terms of membrane species but also with differences in the cytosolic and periplasmic solutions containing macromolecules and ions. There has been a long quest for understanding the effect of ions on the physical and morphological properties of membranes. Here, we elucidate the changes in the mechanical properties of membranes exposed to asymmetric buffer conditions and the associated curvature generation. As a model system, we used giant unilamellar vesicles (GUVs) with asymmetric salt and sugar solutions on the two sides of the membrane. We aspirated the GUVs into micropipettes and attached small beads to their membranes. An optical tweezer was used to exert a local force on a bead, thereby pulling out a membrane tube from the vesicle. The assay allowed us to measure the spontaneous curvature and the bending rigidity of the bilayer in the presence of different ions and sugar. At low sugar/salt (inside/out) concentrations, the membrane spontaneous curvature generated by NaCl and KCl is close to zero, but negative in the presence of LiCl. In the latter case, the membrane bulges away from the salt solution. At high sugar/salt conditions, the membranes were observed to become more flexible and the spontaneous curvature was enhanced to even more negative values, comparable to those generated by some proteins. Our findings reveal the reshaping role of alkali chlorides on biomembranes.

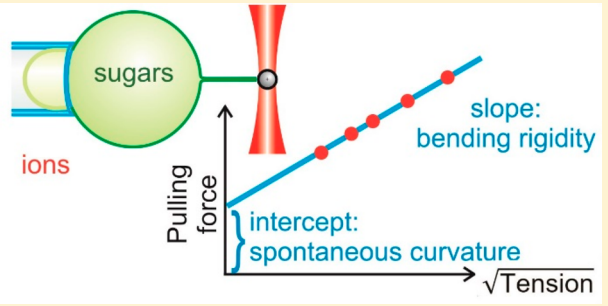

KEYWORDS: *Spontaneous curvature, asymmetric membranes, bending rigidity, membrane nanotubes, protein-free curvature generation, giant vesicle*

Biological membranes are seldom flat but instead often exhibit strongly curved morphology. The shapes of cells and cellular organelles are highly conserved, suggesting that shape and membrane morphology are crucial for life. Deformations from the molecularly preferred curvature cost significant energy, often exceeding 10 k_BT, and yet membrane shape transformations are ubiquitous during cellular and organelle functions. The preferred or spontaneous curvature of membranes is determined by the asymmetry across and within the bilayer,[1,2] and asymmetric conditions across the membrane are a hallmark of cellular life. However, the exact values of the spontaneous biomembrane curvature, and how cells control this important parameter, are poorly understood. Membrane shape changes are often sustained by the action of proteins,[3] but this pathway is costly in terms of energy and molecular material. Ions, however, are abundant in the intra- and extraluminal space of cells and organelles and it is not clear whether and how they affect the membrane morphology and whether cells employ them as a cheap way of controlling membrane shape.

Mammalian cells maintain ion concentration differences by a system of ion channels that enable the cell to regulate the flow of ions across the membrane. Changing sodium and potassium ion concentrations allow nerve impulses to be transmitted down a nerve cell. Ions are responsible for the maintenance of the cellular homeostasis, proper pH, osmotic pressure and water distribution in different fluid compartments of the body.[4] They are also essential for regulating the proper function of the heart and other muscles. These are some examples of important functions of sodium and potassium that make them crucial elements in cells. In addition to sodium and potassium, lithium ions (Li^+) play an important role in metabolism, neural communication, and cell proliferation.[5,6] However, cellular processes controlled by lithium are not thoroughly studied, although low levels of lithium have shown beneficial effect on living organisms; e.g., lithium is a powerful drug in the treatment of manic depression.[7,8]

In conditions where the membrane is exposed to asymmetric concentration of different particles on both sides, the membrane prefers to bulge toward one of the aqueous compartments. This response results from molecular interactions, i.e., either adsorption or depletion. These interactions

Received: September 4, 2018
Revised: November 19, 2018
Published: November 20, 2018

DOI: 10.1021/acs.nanolett.8b03584
Nano Lett. 2018, 18, 7816−7821

may have different effects on the bilayer structure. An adsorbed ion or solute, for example, may insert into the leaflet and push the lipids apart, thereby increasing the effective molecular area. Alternatively, an adsorbed species could also lead to local condensation of lipids, thereby reducing the effective molecular area. This behavior is described by the spontaneous (preferred) curvature of the membrane. It can be positive or negative if the membrane bends away from or toward the lumen, respectively.[1,9] There has been a long quest to understand the effect of ions on the physical and morphological properties of the membrane. Considering the strong ion−lipid interactions supported by abundant evidence for adsorption of ions to the membrane (see, e.g., ref 10 and references therein) and, in particular, the recent findings on the impact of ion trans-membrane asymmetry on the membrane phase state,[11] we set to investigate the effect of ion asymmetry on the mechanical properties of the membranes. We used giant unilamellar vesicles (GUVs) as a model membrane system.[12−14] Their large sizes (in the range of tens of microns) enable us to manipulate the vesicle membranes and visualize the membrane response using optical microscopy. We aimed at investigating and quantifying the effect of Na^+, K^+, and Li^+ and their transmembrane asymmetry on the mechanical properties of phosphatidylcholine (POPC) model membranes.

Experimental Section. *Vesicle Preparation.* GUVs were prepared using the electroformation technique from 2 mM of POPC and 0.1−0.2 mol % of 1,2-dioleoyl-*sn*-glycero-3-phosphoethanolamine-*N*-(cap biotinyl). Additionally, 0.1 mol % Texas Red 1,2-dihexadecanoyl-*sn*-glycero-3-phosphoethanolamine (Texas-Red-DHPE) was added for fluorescence imaging of the vesicles, see section S1 in the Supporting Information.

Experimental Setup. The tube-pulling setup is a combination of the micromanipulation and optical tweezers.[15,16] Micromanipulation was performed using micropipettes of ∼7 μm inner diameters for the aspiration and setting the membrane tension of GUVs (section S2 in the Supporting Information). The optical tweezers setup[16] was calibrated by application of known hydrodynamic forces on the beads and subsequent imaging of the bead position in the trap; see section S3 in the Supporting Information). This calibration was later used to estimate the forces when the bead is displaced from the trap center by the pulled nanotube. Curve fitting and data analysis were preformed using image analysis implemented in MATLAB 2018b[15] and Origin 2018.

Results and Discussion. We prepared GUVs composed of POPC doped with fluorescent lipid by electroformation as described in the Experimental Section and section S1 in the Supporting Information. The vesicles were grown in sugar solutions, which were in this way encapsulated in the GUVs. Subsequent 1:20 dilution of the GUVs in slightly hypotonic salt solutions allowed the study of sugar−salt solution asymmetry on the lipid membrane (the inverse condition of salt inside and sugar outside was not feasible as no suitable vesicles could be produced for the explored salt concentrations). The GUV morphologies in asymmetric solution conditions were imaged with confocal microscopy. In solutions of rather low salt concentrations up to approximately 30 mM of NaCl, the GUVs exhibited mostly smooth, nearly spherical, membranes (Figure 1a, Table 1, condition a). Such vesicle morphologies indicate negligible membrane spontaneous curvature and are typical for GUVs in nearly symmetric solution conditions (data not shown). Strikingly, LiCl solution of similar concentration results in GUVs with highly curved

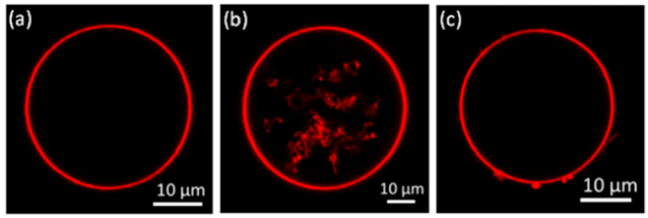

Figure 1. Confocal cross sections of different POPC GUVs with their two leaflets exposed to different solutions of sucrose and salts. GUVs were fluorescently labeled with 0.1 mol % Texas-Red-DHPE and classified as (a) exhibiting no structures, (b) containing numerous nanotubes inside the vesicle, or (c) exhibiting structures (small buds, tubes, folds, or even adhering vesicles) pointing to the outside. Depending on the concentration difference of the salts on the two sides of the membrane, the relative frequency of each morphology changed. The results are summarized in Table 1.

Table 1. Statistics of Internal and External Structures (Compare Figure 1) for GUVs Exposed to Different Solutions of Sucrose and Salt

	asymmetry conditions	no structures	internal structures	external structures
a	low NaCl	82%	6%	2%
b	high NaCl	29%	30%	41%
c	low KCl	34%	39%	27%
d	high KCl	6%	77%	17%
e	low LiCl	20%	69%	10%

[a]GUVs were grown in 54 mM sucrose (inside) and diluted to 28.5 mM NaCl and 2.7 mM sucrose (outside); the total number of vesicles studied for this asymmetry was n = 50. [b]GUVs with 260 mM sucrose inside and 142.5 mM NaCl plus 13 mM sucrose outside; n = 130. [c]GUVs with 114 mM sucrose inside and 57 mM KCl plus 5.7 mM sucrose outside; n = 58. [d]GUVs with 260 mM sucrose inside and 142.5 mM KCl plus 13 mM sucrose outside; n = 135. [e]GUVs with 54 mM sucrose inside and 28.5 mM LiCl plus 2.7 mM sucrose outside; n = 85. For all measurements, the given fractions have an uncertainty of about 15%. The observed external structures include small buds and tubes, but also adhering vesicles.

membrane segments (nanotubes) pointing to the vesicle interior with diameters below the optical resolution (Figure 1b, Table 1, condition e). Direct observations of individual vesicles upon solution exchange showed the formation of the tubes induced by LiCl asymmetry; see Figure S1 in the Supporting Information. They were reminiscent of cylindrical and necklace-like tubes observed in studies with membranes exposed to polymer asymmetry.[17,18] Increasing NaCl and KCl concentrations up to physiological levels (150 mM) leads to a similar tendency for inward pointing nanotubes (Table 1, conditions b and d); note that the fraction of external structures also increases, which results from not only outward membrane protrusions but also adhesion of smaller vesicles. In principle, optical observation of tubes or buds allows for direct quantification of the membrane spontaneous curvature.[2,18,19] However, adhesion of small vesicles to the GUVs (Figure 1c, which would be counted as external structures in Table 1), most prominent at high NaCl concentrations, interferes with clear assessment of the spontaneous curvature from such morphological studies alone. High LiCl concentrations were not investigated due to the strong adhesion of GUVs to each other.

To quantify the spontaneous curvature, we applied the more quantitative method of pulling of membrane nanotubes from

DOI: 10.1021/acs.nanolett.8b03584
Nano Lett. 2018, 18, 7816−7821

the GUV membrane (see, e.g., refs 15 and 20). In this method, GUVs are aspirated with a micropipette, which controls the membrane tension Σ_{asp} of the vesicles by changing the hydrostatic pressure difference applied by changing the height of a water reservoir connected to the pipet, see section S2 in the Supporting Information. A 2 μm streptavidin bead trapped by optical tweezers was stuck to the vesicle and used to pull a membrane nanotube with 10 μm length from the GUV. In this configuration, the pulling force can be estimated from the position of the bead in the optical trap which was measured by optical microscopy; see section S3 in the Supporting Information. The pulling force f for an outward tube is given by[1,15]

$$f = 2\pi\sqrt{2\kappa\Sigma_{asp}} - 4\pi\kappa m \quad (1)$$

where κ is the bending rigidity and m is the membrane spontaneous curvature. Thus, by measuring the force for different membrane tension set by the pipet, one can deduce the bending rigidity form the slope of the data (first term in eq 1) and the spontaneous curvature from the intercept (second term). Figure 2 represents the experiment schematic and images of vesicles with a pulled membrane nanotube.

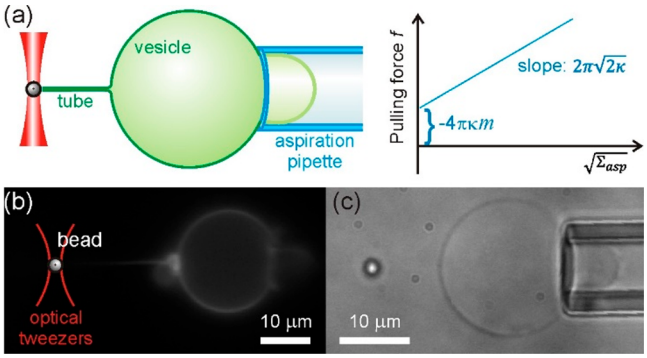

Figure 2. Experimental assay for pulling out a nanotube from a GUV: (a) sketch of the setup and principle of measurement and (b) epifluorescence and (c) bright-field images of an aspirated vesicle with a pulled tube.

The streptavidin-coated beads were injected into the experimental chamber locally via a syringe and were moved into the proximity of a GUV using the optical tweezers (see Experimental Section and section S2). A freely fluctuating GUV was aspirated into the glass capillary, a bead stuck to it, and a nanotube was pulled out by translating the vesicle away. Tube pulling experiments started with low concentration of NaCl outside the membrane, which was identified as the minimal salt concentration where bead−membrane adhesion was still efficient. As determined in the morphological studies of GUVs, this concentration was used further as a reference to compare our data to conditions that induce higher membrane asymmetry. Note that controls with symmetric sugar conditions were not possible as beads were not adhering to the membrane and thus tubes could not be pulled in the absence of salt. In all experimental conditions, vesicles were studied at suction pressures between ∼20 and ∼49 Pa. The membrane tension of the vesicles at each pressure could be assessed from the geometry of the aspirated vesicle and the applied pressure difference; see Supporting Information section S2. By careful calibration of the optical trap, the force exerted on the bead holding the nanotubes was determined from the optically measured bead displacement (see Experimental Section and Supporting Information sections S3 and S4). When tube pulling forces were measured, the trapped bead was displaced to the edge of the trap, i.e., away from the linear region of the trapping force field. This allowed us, for the same trap beam power, to measure higher forces than when the linear trapping force region was used. This is an advantageous approach as in this way the heating of the bead and the attached membrane is reduced.[21,22] Moreover, considering possible variations of sizes of the trapped latex beads, we calibrated the trap stiffness for each individual bead before using it for pulling tubes. An approach combining the equipartition method and viscous drag method was used (see Supporting Information section S4).

By fitting all force vs tension data points to a linear fit following eq 1, the mean bending rigidity of vesicles with low NaCl asymmetry (Figure 3a) was estimated as 34.79 ± 0.81 k_BT. This value is well within the range of data reported for POPC membranes[23] and in particular for POPC vesicles in the presence of NaCl as measured from fluctuation analysis.[24,25] The spontaneous curvature of the membrane determined from the y-axis intercept of the fitted line was found to be 0.66 ± 0.30 μm^{-1}; note that fitting individual measurements and subsequent averaging yields 0.09 ± 0.68 μm^{-1}; see Table S1. This spontaneous curvature is negligible (comparable to the mean curvature of the GUVs), which is consistent with the spherical nontubulated morphologies observed in the microscopy images statistics (Table 1).

Identical experiments were performed on vesicles exposed to high asymmetry of physiological concentration (150 mM) of NaCl outside and isotonic sucrose inside the vesicles. Six vesicles were studied in this condition and the mean bending rigidity was estimated to be 23.60 ± 0.60 k_BT (Figure 3a). Comparing the bending rigidity in the two explored NaCl conditions, we conclude that the bending rigidity decreases by increasing NaCl (and sugar) concentration, confirming a trend reported in refs 24 and 25 (note that salts are reported to rigidify bilayer stacks (see, e.g., ref 26), which underlies the difference in the behavior of single membranes as in giant vesicles and multiple layers as in multilayered systems, each exploring lipid-to-ion ratios that differ by orders of magnitude). As a reminder, at high salt asymmetry, the sugar concentration inside the vesicles is also increased and sugars have been also shown to decrease the membrane bending rigidity (see overview in ref 23) presumably because of membrane thinning in this concentration range.[27] It can be also seen from Figure 3a that while the intercept of the linear fit under low asymmetry is zero within the fitting accuracy (blue shaded region), the intercept at high NaCl asymmetry implies nonzero spontaneous curvature. We estimated this negative spontaneous curvature as −8.74 ± 0.50 μm^{-1}, again consistent with the spontaneous appearance of membrane tubes with diameters below optical resolution (<0.5 μm) observed in the morphology studies (Table 1). The values obtained for the spontaneous curvature imply that it would stabilize cylindrical tubes with diameters around 110 nm. Measuring the tube diameter using fluorescence intensity as done in refs 28 and 29 was not feasible, as our microscope setup was equipped for epifluorescence only where bleaching poses a problem.

In some of the experiments at high NaCl asymmetry, the measured spontaneous curvature was found close to zero, but upon inspection of the vesicle population with phase contrast microscopy and employing an encapsulated water-soluble

DOI: 10.1021/acs.nanolett.8b03584
Nano Lett. 2018, 18, 7816−7821

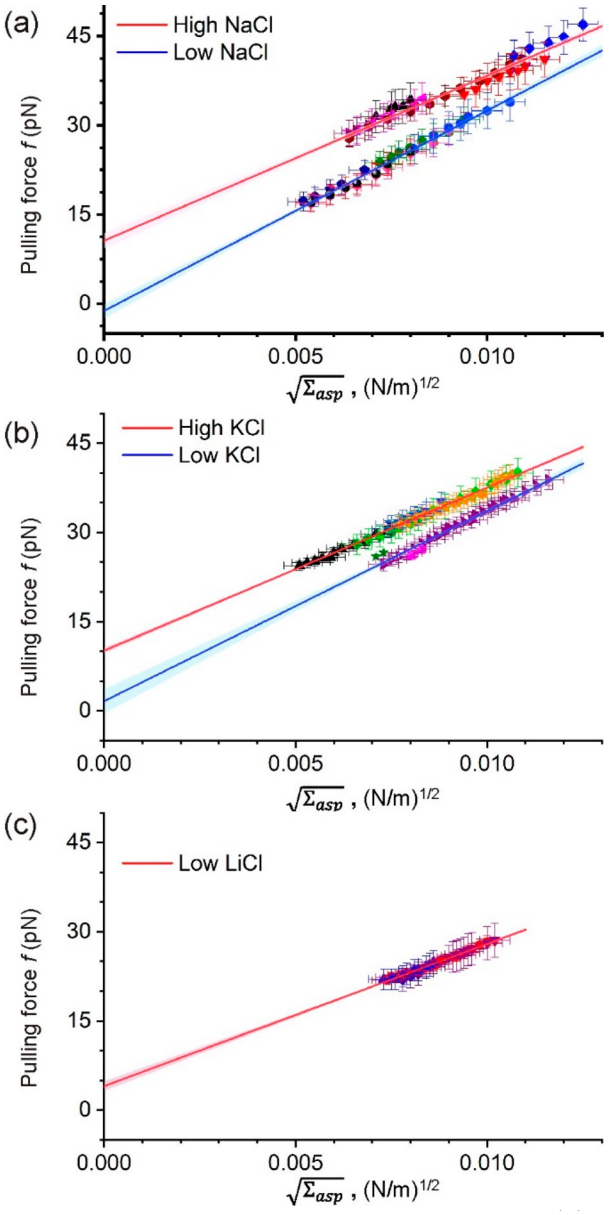

Figure 3. Results for out tubes showing the pulling force (f) vs the square root of the membrane tension Σ_{asp} for vesicles exposed to low asymmetry (blue linear fits) and high asymmetry (red linear fits) of sucrose inside and (a) NaCl outside, (b) KCl outside, and (c) LiCl outside the vesicles (the respective solution concentrations are given in the caption of Table 1). Differently colored symbols reflect measurements on different vesicles from different preparations. The solid lines are fits following eq 1, yielding the material properties of the membrane, i.e., the bending rigidity and spontaneous curvature as schematically illustrated in Figure 2a.

fluorophore, we found that this is because vesicles have leaked and the asymmetry has been compromised; see Supporting Information section S5.

Similar experiments were performed for asymmetric KCl solutions. Concentration-wise, the low-asymmetry condition here does not correspond to that of low NaCl asymmetry as higher concentrations of KCl were required to ensure the beads sticking to the membrane. The respective bending rigidity values were 31.87 ± 1.08 k_BT and 23.11 ± 0.24 k_BT for low and high asymmetries, indicating softening of the membrane by KCl as observed for NaCl. Similarly, increasing KCl asymmetry was found to induce significant negative spontaneous curvature on the membranes; see Figure 3b and data summarized in Table 2. To restate, the bending rigidity

Table 2. Mean Values and Standard Deviations of the Bending Rigidity and the Spontaneous Curvature of Vesicle Membranes Exposed to Asymmetric Solutions of Sucrose and Salt As Described in the Caption of Table 1[a]

condition	κ (k_BT)	m (μm^{-1})
low NaCl	34.79 ± 0.81	0.66 ± 0.30
high NaCl	23.60 ± 0.60	−8.74 ± 0.50
low KCl	31.87 ± 1.08	−1.00 ± 0.59
high KCl	23.11 ± 0.24	−8.47 ± 0.24
low LiCl	17.52 ± 0.34	−4.45 ± 0.45

[a]Each value is obtained from a fit to all data for a given buffer composition. For values obtained from individual fits and subsequent averaging, see section S6 and Tables S1−S5 in the Supporting Information. The exact salt and sugar concentration conditions are given in Table 1.

and spontaneous curvature values are comparable for vesicles exposed to two different salts, i.e., NaCl and KCl in two different concentration ranges; i.e., each of these alkali chlorides affects the membrane similarly in terms of softening and curvature generation.

Finally, we also explored the effect of LiCl asymmetry. Even though physiological concentrations of lithium are in the (sub)millimolar range, studies on axonal remodeling and growth cone spreading (see, e.g., ref 30) explore concentrations on the order of 10 mM. To compare our results on NaCl asymmetry, we explored LiCl asymmetry at the same ion concentration; see Figure 3C and Table 1 for exact conditions. Even at this low LiCl concentration the bending rigidity is considerably decreased and a significant negative spontaneous curvature was measured consistent with microscopy observations (Table 1). All experiments are summarized in Table 2.

To confirm the effect of the salts on the lipid bilayers, the membrane bending rigidity was also measured via fluctuation analysis;[31] see section S7 in the Supporting Information. The values of bending rigidity were estimated to be 29.8 ± 3.7 k_BT and 19.2 ± 5.0 k_BT for vesicles exposed to low asymmetry of KCl and LiCl, respectively. These results are in good agreement with the bending rigidity values obtained from tube pulling experiments in Table 2.

Conclusions. In this paper, we used a combination of optical tweezers and micropipette manipulation of giant vesicles to pull out lipid nanotubes and measure fundamental mechanical properties of the membranes. We focused on the effect of ionic asymmetry across the membrane as present in cells. The vesicles were exposed to different concentrations of sucrose (inside) and three different types of salts (outside), namely, NaCl, KCl, and LiCl. Measurements of the tube pulling force and membrane tension of the vesicles, allowed us to assess the bending rigidity and spontaneous curvatures generated in the above conditions. The magnitude for the spontaneous curvature generated at high NaCl and KCl asymmetry is lower than values measured on membranes exposed to BAR domain proteins[32] (m^{-1} ∼ 20−100 nm) and comparable to that of membranes with asymmetric distribution of gangliosides,[15,33] polymers,[18] and more importantly, divalent ions[34,35] (m^{-1} ∼ 100−500 nm). The sign of the spontaneous curvature generated by calcium reported in refs 34 and 35 is

DOI: 10.1021/acs.nanolett.8b03584
Nano Lett. 2018, 18, 7816−7821

controversial; one group reported that binding of calcium ions to these membranes generates positive spontaneous curvature,[34] whereas measurements of another group at the same conditions yielded negative spontaneous curvature.[35] Our results for NaCl and KCl corroborate negative spontaneous curvature at high salt concentration. Indeed, similarly to direct calcium-induced inward tubulation shown in ref 36, we do observe more abundant internal tubes in these vesicles (Table 1). Thus, in the presence of salt solutions, vesicle membranes tend to curve away from the exterior salt solution attaining a negative spontaneous curvature. Presumably, the ions that adsorb to the membrane lead to local condensation of lipids, thereby reducing the effective molecular area of the leaflet exposed to them.

Interestingly, increasing salt asymmetries correlated with the change in the values of both the bending rigidity and spontaneous curvature. Generally, sugars are thought to soften membranes via thinning of the bilayers[27] while alkali ions, except for lithium, are considered as not interacting with the membrane.[37] As suggested by simulations and NMR data,[37] we thus speculate that the spontaneous curvature is generated by sodium and potassium ion depletion from the bilayer (outer leaflet) while the adsorbed lithium (similarly to the effect of calcium) leads to local condensation of lipids, thereby reducing the effective molecular area of the leaflet exposed to them. From fluorescence lifetime measurements[38] we attempted to distinguish the condensing effect of lithium ions from the depletion of sodium and potassium ions from the membrane; see section S8 in the Supporting Information. The lifetime of the used dye was altered only in the presence of LiCl (corresponding to the low LiCl asymmetry condition explored here) but not in the presence of NaCl and KCl solutions (in both high and low asymmetry conditions). We thus conclude that our speculations for the depletion of sodium and potassium ions from the membrane as well as for the condensing effect of lithium are reasonable. Presumably, molecular dynamics simulation studies will be able to further characterize the mechanism of curvature generation by monovalent salt asymmetry. In our experiments, the effect of the ions may also be enhanced by thinning of the monolayer facing the sugar solution (sugars are believed to laterally expand the leaflet[27]), all together driving the generation of the negative spontaneous curvature. One significant result to be emphasized here is that the bending rigidity and negative curvature generated by both NaCl and KCl are comparable. While the vesicle membrane has almost zero spontaneous curvature at low concentration of these salts, low concentration of LiCl induces a negative curvature that is approximately equivalent to half the value measured for the high asymmetry conditions with NaCl and KCl. In a number of studies, lithium has been shown to have an inhibitory role on proteins (see, e.g., refs 8, 30, and 39 and references therein), leading to the conclusion that neuronal remodeling is predominantly governed by the activity of these proteins. Here, we show that biomembrane reshaping might result not solely from protein inhibition by lithium but also by the direct action of LiCl on membrane rigidity and spontaneous curvature resulting from the applied asymmetric solutions.

■ ASSOCIATED CONTENT

Supporting Information

The Supporting Information is available free of charge on the ACS Publications website at DOI: 10.1021/acs.nanolett.8b03584.

Discussion of vesicle preparation and observation, micropipette manipulation, and optical trapping and calibration (including figures of epifluorescence images of one GUV; apparatus setup; trapped particle image, trajectory, and displacement; trap stiffness vs camera exposure time and particle number; and bead off-center displacement); tables of bending rigidity and spontaneous curvature data from individual vesicles; fluctuation analysis; fluorescence lifetime measurements (PDF)

■ AUTHOR INFORMATION

Corresponding Author

*Rumiana Dimova. E-mail: dimova@mpikg.mpg.de.

ORCID

Reinhard Lipowsky: 0000-0001-8417-8567

Rumiana Dimova: 0000-0002-3872-8502

Present Address

§Department of Cell Biology and Physiology, Washington University School of Medicine, St. Louis, MO 63110, USA.

Author Contributions

R.D., J.S., and M.K. designed the experiments. R.L. proposed the project. M.K. and J.S. performed the experiments. R. Dimova, D.R., J.S., M.K., and R. Dasgupta developed the trap calibration assay. All authors wrote the manuscript.

Notes

The authors declare no competing financial interest.

■ ACKNOWLEDGMENTS

This work is part of the MaxSynBio consortium which was jointly funded by the Federal Ministry of Education and Research of Germany and the Max Planck Society.

■ REFERENCES

(1) Lipowsky, R. Spontaneous tubulation of membranes and vesicles reveals membrane tension generated by spontaneous curvature. *Faraday Discuss.* **2013**, *161*, 305−331.

(2) Bassereau, P.; Jin, R.; Baumgart, T.; Deserno, M.; Dimova, R.; Frolov, V. A.; Bashkirov, P. V.; Grubmüller, H.; Jahn, R.; Risselada, H. J.; Johannes, L.; Kozlov, M. M.; Lipowsky, R.; Pucadyil, T. J.; Zeno, W. F.; Stachowiak, J. C.; Stamou, D.; Breuer, A.; Lauritsen, L.; Simon, C.; Sykes, C.; Voth, G. A.; Weikl, T. R. The 2018 biomembrane curvature and remodeling roadmap. *J. Phys. D: Appl. Phys.* **2018**, *51* (34), 343001.

(3) Zimmerberg, J.; Kozlov, M. M. How proteins produce cellular membrane curvature. *Nat. Rev. Mol. Cell Biol.* **2006**, *7*, 9.

(4) Pohl, H. R.; Wheeler, J. S.; Murray, H. E. Sodium and Potassium in Health and Disease. In *Interrelations between Essential Metal Ions and Human Diseases*; Sigel, A., Sigel, H., Sigel, R. K. O., Eds.; Springer: Dordrecht The Netherlands, 2013; pp 29−47.

(5) Shahzad, B.; Mughal, M. N.; Tanveer, M.; Gupta, D.; Abbas, G. Is lithium biologically an important or toxic element to living organisms? An overview. *Environ. Sci. Pollut. Res.* **2017**, *24* (1), 103−115.

(6) Williams, R.; Ryves, W. J.; Dalton, E. C.; Eickholt, B.; Shaltiel, G.; Agam, G.; Harwood, A. J. A molecular cell biology of lithium. *Biochem. Soc. Trans.* **2004**, *32*, 799−802.

(7) Pasternak, C. A. *Monovalent Cations in Biological Systems*; CRC Press, 1990.

DOI: 10.1021/acs.nanolett.8b03584
Nano Lett. 2018, 18, 7816−7821

(8) Klein, P. S.; Melton, D. A. A molecular mechanism for the effect of lithium on development. *Proc. Natl. Acad. Sci. U. S. A.* **1996**, *93* (16), 8455.
(9) Lipowsky, R. Coupling of bending and stretching deformations in vesicle membranes. *Adv. Colloid Interface Sci.* **2014**, *208*, 14−24.
(10) Klasczyk, B.; Knecht, V.; Lipowsky, R.; Dimova, R. Interactions of Alkali Metal Chlorides with Phosphatidylcholine Vesicles. *Langmuir* **2010**, *26* (24), 18951−18958.
(11) Kubsch, B.; Robinson, T.; Lipowsky, R.; Dimova, R. Solution Asymmetry and Salt Expand Fluid-Fluid Coexistence Regions of Charged Membranes. *Biophys. J.* **2016**, *110* (12), 2581−2584.
(12) Dimova, R.; Aranda, S.; Bezlyepkina, N.; Nikolov, V.; Riske, K. A.; Lipowsky, R. A practical guide to giant vesicles. Probing the membrane nanoregime via optical microscopy. *J. Phys.: Condens. Matter* **2006**, *18* (28), S1151−S1176.
(13) Walde, P.; Cosentino, K.; Engel, H.; Stano, P. Giant Vesicles: Preparations and Applications. *ChemBioChem* **2010**, *11* (7), 848−865.
(14) Dimova, R. Giant Vesicles: A Biomimetic Tool for Membrane Characterization. In *Advances in Planar Lipid Bilayers and Liposomes*, Iglič, A., Ed.; Academic Press, 2012; Vol. *16*, pp 1−50.
(15) Dasgupta, R.; Miettinen, M. S.; Fricke, N.; Lipowsky, R.; Dimova, R. The glycolipid GM1 reshapes asymmetric biomembranes and giant vesicles by curvature generation. *Proc. Natl. Acad. Sci. U. S. A.* **2018**, *115*, 5756−5761.
(16) Kraikivski, P.; Pouligny, B.; Dimova, R. Implementing both short- and long-working-distance optical trappings into a commercial microscope. *Rev. Sci. Instrum.* **2006**, *77* (11), 113703.
(17) Li, Y.; Lipowsky, R.; Dimova, R. Membrane nanotubes induced by aqueous phase separation and stabilized by spontaneous curvature. *Proc. Natl. Acad. Sci. U. S. A.* **2011**, *108* (12), 4731−4736.
(18) Liu, Y.; Agudo-Canalejo, J.; Grafmüller, A.; Dimova, R.; Lipowsky, R. Patterns of Flexible Nanotubes Formed by Liquid-Ordered and Liquid-Disordered Membranes. *ACS Nano* **2016**, *10* (1), 463−474.
(19) Nikolov, V.; Lipowsky, R.; Dimova, R. Behavior of giant vesicles with anchored DNA molecules. *Biophys. J.* **2007**, *92* (12), 4356−4368.
(20) Sorre, B.; Callan-Jones, A.; Manneville, J. B.; Nassoy, P.; Joanny, J. F.; Prost, J.; Goud, B.; Bassereau, P. Curvature-driven lipid sorting needs proximity to a demixing point and is aided by proteins. *Proc. Natl. Acad. Sci. U. S. A.* **2009**, *106* (14), 5622−5626.
(21) Liu, Y.; Cheng, D. K.; Sonek, G. J.; Berns, M. W.; Chapman, C. F.; Tromberg, B. J. Evidence for localized cell heating induced by infrared optical tweezers. *Biophys. J.* **1995**, *68* (5), 2137−2144.
(22) Bolognesi, G.; Friddin, M. S.; Salehi-Reyhani, A.; Barlow, N. E.; Brooks, N. J.; Ces, O.; Elani, Y. Sculpting and fusing biomimetic vesicle networks using optical tweezers. *Nat. Commun.* **2018**, *9* (1), 1882.
(23) Dimova, R. Recent developments in the field of bending rigidity measurements on membranes. *Adv. Colloid Interface Sci.* **2014**, *208* (0), 225−234.
(24) Bouvrais, H. Mechanical properties of giant vesicle membranes investigated by flickering technique. *Ph.D. thesis*, University of Southern Denmark, Odense, 2011.
(25) Bouvrais, H. Bending Rigidities of Lipid Bilayers: Their Determination and Main Inputs in Biophysical Studies. In *Advances in Planar Lipid Bilayers and Liposomes*; Iglič, A., Ed.; Academic Press, 2012; Vol. *15*, pp 1−75.
(26) Pabst, G.; Hodzic, A.; Strancar, J.; Danner, S.; Rappolt, M.; Laggner, P. Rigidification of neutral lipid bilayers in the presence of salts. *Biophys. J.* **2007**, *93* (8), 2688−2696.
(27) Andersen, H. D.; Wang, C. H.; Arleth, L.; Peters, G. H.; Westh, P. Reconciliation of opposing views on membrane-sugar interactions. *Proc. Natl. Acad. Sci. U. S. A.* **2011**, *108* (5), 1874−1878.
(28) Sorre, B.; Callan-Jones, A.; Manzi, J.; Goud, B.; Prost, J.; Bassereau, P.; Roux, A. Nature of curvature coupling of amphiphysin with membranes depends on its bound density. *Proc. Natl. Acad. Sci. U. S. A.* **2012**, *109* (1), 173−178.
(29) Aimon, S.; Callan-Jones, A.; Berthaud, A.; Pinot, M.; Toombes, G. E. S.; Bassereau, P. Membrane Shape Modulates Transmembrane Protein Distribution. *Dev. Cell* **2014**, *28* (2), 212−218.
(30) Hall, A. C.; Lucas, F. R.; Salinas, P. C. Axonal Remodeling and Synaptic Differentiation in the Cerebellum Is Regulated by WNT-7a Signaling. *Cell* **2000**, *100* (5), 525−535.
(31) Gracià, R. S.; Bezlyepkina, N.; Knorr, R. L.; Lipowsky, R.; Dimova, R. Effect of cholesterol on the rigidity of saturated and unsaturated membranes: fluctuation and electrodeformation analysis of giant vesicles. *Soft Matter* **2010**, *6* (7), 1472−1482.
(32) McMahon, H. T.; Gallop, J. L. Membrane curvature and mechanisms of dynamic cell membrane remodelling. *Nature* **2005**, *438* (7068), 590−596.
(33) Bhatia, T.; Agudo-Canalejo, J.; Dimova, R.; Lipowsky, R. Membrane Nanotubes Increase the Robustness of Giant Vesicles. *ACS Nano* **2018**, *12* (5), 4478−4485.
(34) Simunovic, M.; Lee, K. Y. C.; Bassereau, P. Celebrating Soft Matter's 10th anniversary: screening of the calcium-induced spontaneous curvature of lipid membranes. *Soft Matter* **2015**, *11* (25), 5030−5036.
(35) Graber, Z. T.; Shi, Z.; Baumgart, T. Cations induce shape remodeling of negatively charged phospholipid membranes. *Phys. Chem. Chem. Phys.* **2017**, *19* (23), 15285−15295.
(36) Ali Doosti, B.; Pezeshkian, W.; Bruhn, D. S.; Ipsen, J. H.; Khandelia, H.; Jeffries, G. D. M.; Lobovkina, T. Membrane Tubulation in Lipid Vesicles Triggered by the Local Application of Calcium Ions. *Langmuir* **2017**, *33* (41), 11010−11017.
(37) Catte, A.; Girych, M.; Javanainen, M.; Loison, C.; Melcr, J.; Miettinen, M. S.; Monticelli, L.; Määttä, J.; Oganesyan, V. S.; Ollila, O. H. S.; Tynkkynen, J.; Vilov, S. Molecular electrometer and binding of cations to phospholipid bilayers. *Phys. Chem. Chem. Phys.* **2016**, *18* (47), 32560−32569.
(38) Packard, B. S.; Wolf, D. E. Fluorescence lifetimes of carbocyanine lipid analogs in phospholipid bilayers. *Biochemistry* **1985**, *24* (19), 5176−5181.
(39) Williams, R. S. B.; Cheng, L.; Mudge, A. W.; Harwood, A. J. A common mechanism of action for three mood-stabilizing drugs. *Nature* **2002**, *417*, 292.

DOI: 10.1021/acs.nanolett.8b03584
Nano Lett. 2018, 18, 7816−7821

Supporting information

Asymmetric ionic conditions generate large membrane curvatures

Marzieh Karimi[1], Jan Steinkühler[1], Debjit Roy[1,2], Raktim Dasgupta[1,3], Reinhard Lipowsky[1] and Rumiana Dimova[1]*

[1]Department of Theory and Bio-Systems, Max Planck Institute of Colloids and Interfaces, Science Park Golm, 14424 Potsdam, Germany

[2]Present address: Department of Cell Biology and Physiology, Washington University School of Medicine, St. Louis, Missouri 63110, USA

[3]Laser Biomedical Applications Section, Raja Ramanna Centre for Advanced Technology, 452013 Indore, India

*Address for correspondence: dimova@mpikg.mpg.de

Section S1. Preparation and observation of giant unilamellar vesicles (GUVs)

GUVs were prepared using the electroformation technique[1]. 2 mM solution of 1-palmitoyl-2-oleoyl-sn-glycero-3-phosphatidylcholine (POPC) containing a fraction (0.1 - 0.2 mol%) of 1,2-dioleoyl-*sn*-glycero-3-phosphoethanolamine-N-(cap biotinyl) in chloroform was prepared. Both lipids were purchased from Avanti Polar Lipids. Additionally, 0.1 mol% Texas Red 1,2-dihexadecanoyl-sn-glycero-3-phosphoethanolamine (Texas-Red-DHPE) or 0.2 mol% DiI ($DiIC_{18}(3)$; 1,1′-dioctadecyl-3,3,3′,3′-tetramethylindocarbocyanine, Thermo Fisher Scientific) was added for fluorescence imaging of the vesicles. Typically, 4 µl of the lipid solution was spread onto the electrically conductive side of indium tin oxide (ITO)-coated glass plates (Praezisions Glas & Optik, Iserlohn, Germany) and dried under vacuum for at least 30 minutes to remove the organic solvents. The amount of lipid solution was optimized for GUV yield to prevent vesicles attaching to each other. The glass plates were put against a 2 mm thick Teflon spacer to form a closed chamber held together by office clamps. The swelling solution (as indicated in the text) was added and a sinusoidal AC electric field at 10 Hz was applied for electro swelling of the lipid films. The voltage was held steady at 1.06 V_{rms} for 60 min. This voltage was measured at the ITO-coated glass plates. Once the vesicles were formed, they were diluted in the solution of interest (see main text) and transferred to the observation chambers to be used under the microscopes for further investigations. Both the drying and electro swelling were carried out at room temperature (23° C) at which the lipid bilayer is in the fluid phase. Vesicles were imaged using confocal microscope (SP5 DMI 6000, Leica Microsystems Heidelberg GmbH, Germany) or by the optical tweezers set up[2] built around a motorized inverted microscope (Axiovert 200M, Zeiss). For confocal imaging and statistics of vesicle morphologies, only vesicles with diameters larger than 15 µm were considered to correspond to the size range examined with micropipette manipulation and fluctuation analysis. The whole vesicle surface (and not only equatorial confocal cross sections) was explored for structures. The data in Table 1 in the main text is averaged over different vesicle preparations.

We also explored the response of individual vesicles subjected directly to exchange of the external solution. The GUVs labeled with 0.2 mol % DiI were prepared in 54 mM sucrose and observed under the epifluorescence microscope. The vesicles appeared spherical mostly without any internal or external structures. In the observation chamber, 50 µl GUVs suspension was directly diluted (20 times) with 30 mM LiCl solution to a final concentration 28 mM LiCl +2.7 mM sucrose outside the vesicles. Right after dilution, we tracked a vesicle to explore the morphological changes induced by the addition of LiCl. Figure S1 shows the formation of internal structures in the presence of LiCl implying the generation of negative spontaneous curvature.

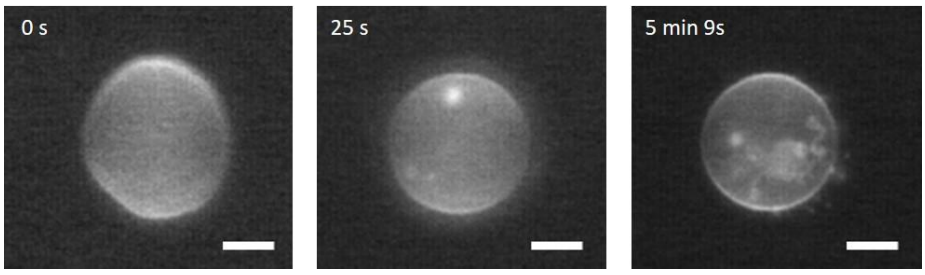

Figure S1: Epifluorescence images of one GUV prepared in 54 mM sucrose solution shortly after being exposed to LiCl solution of 28 mM final concentration in the chamber. The respective time stamps after starting the

observations (~10-20 seconds after having introduced the LiCl solution in the observation chamber) are indicated in the upper left corners of the images. With time, the vesicle develops internal tubes. Scale bar, 10 μm.

Section S2. Micropipette manipulation and aspiration of GUVs

Micromanipulation of GUVs was performed in a homemade experimental chamber. The chamber was built from two parallel 160 μm thick glass coverslips (24×50 mm^2 and 24×24 mm^2) separated by a U-shaped Teflon spacer with internal dimensions of 20 mm in width, length of 24 mm and height of 4 mm and an opening from one side in order to insert the micropipette to the chamber horizontally (Fig. S2). To deal with bead sedimentation in the chamber (beads then can stick to the bottom glass) and possible pollution of their surface by lipid aggregates floating in the solution, they were injected when needed via a needle in a hole on one side of the spacer using a syringe operated by a microinjector (model: IM-9B, Narishige Japan).

Micropipettes were pulled from borosilicate capillaries (1B100-4, World Precision Instruments Inc.) using a pipette puller (Sutter Instruments, Novato, CA) and then were cut using a microforge (Narishige, Tokyo, Japan) at desired inner diameters of ~7 μm. The adhesion of vesicle membranes to the pipette was prevented by incubation of the pipette tips in 5 mg/mL aqueous solution of BSA (Bovine Serum Albumin, Sigma Aldrich, Darmstadt, Germany). After the incubation, the micropipette was rinsed two or three times with the working solution in order to remove the BSA solution from the capillary tip. Moreover to prevent adhesion of the vesicles to the surfaces of the cover glass, the chamber was coated with 3-5 mg/mL ß-casein (Sigma) and then rinsed similarly with the experimental buffer. Additionally, the chamber was then prefilled with a solution containing GUVs for about 45 minutes and the solution discarded. In this way, areas not properly coated with casein were coated with membrane thus preventing adhesion and bursting of the fresh vesicles (which was often observed when working at high salt concentrations). This step also helped to remove the unbound ß-casein. Finally, we refilled the chamber with a fresh GUVs solution.

The chamber was mounted on the microscope and a single micropipette was inserted into the sample chamber using a three-dimensional micromanipulator system (Narishige Corp, Japan) clamped on the microscope (Fig. S2A). Equilibrium height of the water reservoir corresponding to zero pressure across the pipette tip was set when there was no flow of small particles in the vicinity of the tip. The aspiration pressure in the micropipette was controlled by changing the height of the reservoir mounted on a linear translational stage (M-531.PD; Physik Instrumente, Germany). The respective membrane tension Σ_{asp} was calculated from

$$\Sigma_{asp} = \Delta P \frac{R_{sp} R_{pip}}{2\left(R_{sp} - R_{pip}\right)}$$

where ΔP is the suction pressure, R_{sp} and R_{pip} are respectively the radii of the spherical vesicle and the micropipette. To apply the Laplace equation, the projection length of the vesicle must exceed the radius of the micropipette. Therefore we selected a well deflated vesicle and aspirated it with a high value of the aspiration pressure. This step of vesicle prestressing[3] ensured pulling out vesicle area stored in membrane folds and tubes. Then we decreased the pressure up to a point at which the micropipette could still hold the vesicle and the membrane tension was small. Few seconds after the attachment of a trapped bead to the vesicle, we slightly increased the distance between the bead and

vesicle membrane to attain a desired length of the tube (~10 µm). This length was kept constant during the whole experiment. Membrane tension was then increased slightly and for each tension the position of the bead relative to the trap center was recorded (500-1000 frames) by video microscopy. Note that it is important to set the zero reference pressure in the micropipette before each experiment on a new vesicle to compensate (small) changes in solution osmolarity by evaporation. This can be achieved by detecting the absence of a bead movement around the micropipette. All experiments were performed at room temperature, 23±1◦C.

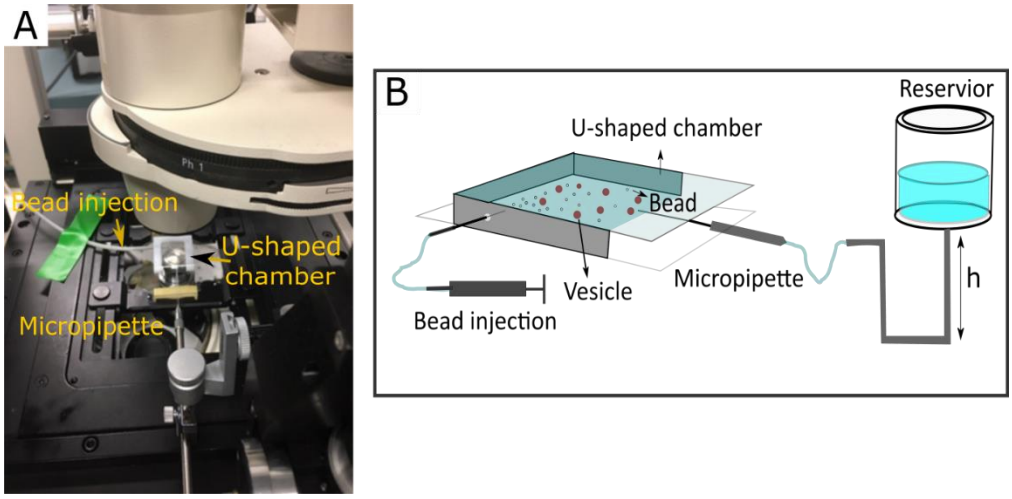

Figure S2: Observation chamber for micropipette manipulation. (A) A snapshot of the chamber at the microscope stage. (B) Schematic representation of the chamber and micropipette aspiration setup.

Section S3. Optical tweezers and force measurement

The optical tweezers was built around a motorized inverted microscope (Axiovert 200M, Zeiss) and a tightly focused laser beam from a 1064 nm continuous wave Nd:YAG laser (Spectra Physics, USA). Typical laser power used in our experiments was ~155 mW at the sample. Images were captured by an EMCCD camera (ImagEM, Hamamatsu Corp) at more than 40 frames per second. The optical tweezers was used to trap streptavidin-coated microspheres (Polyscience Inc., Cat #24160) with a diameter of ~1.9 µm. These microspheres can be attached to the biotinylated lipid membranes, which enables the manipulation of the vesicles in order to pull out tubes. When such tube is formed, the position of the bead is slightly displaced from the trap center. For small displacements, the force exerted by the tube is proportional to the bead displacement from the trap center. This force can be estimated by

$$f = -K(x - x_0) \tag{S1}$$

where $x - x_0$ is the displacement of the trapped bead from the trap center (x_0), when a tube is pulled and K is the trap stiffness. Quantitative use of the optical tweezers relies on accurate calibration of the trap stiffness which in our work is determined using the viscous drag method and the equipartition theorem (Section S4). In both methods, the bead was imaged using the EMCCD camera and its position was determined using centroid tracking algorithm[4] written in MATLAB (Mathworks Inc). All measurements were performed at a height of ~20 µm above the glass boundary of the sample chamber. The streptavidin-coated beads were washed to remove additives and residuals that

could interfere with the binding reactions of beads with GUVs. In this regard, the beads were spun down and washed three times using centrifuge at 13200 rpm for 3 min.

Section S4. Calibration of optical tweezers

When measuring tube pulling forces, the trapped bead was allowed to get displaced to the edge of the trap, i.e. away from the linear region of the trapping force field. This allowed us to assess higher forces (for the same trap beam power) than when using the linear trapping force region, resulting in reduced heating of the bead and attached vesicle. Moreover, considering possible variations of sizes of the trapped latex beads (see below) we calibrated the trap stiffness for each individual bead before using it for pulling tubes. An approach combining the equipartition theorem method and viscous drag method was used.

According to the equipartition theorem (ET), the trap stiffness is given by:

$$K_{ET} = \frac{k_B T}{\langle x^2 \rangle} \tag{S2}$$

where k_B is the Boltzmann constant, T is the absolute temperature and $\langle x^2 \rangle$ is the statistical variance in the trapped particle position resulting from the Brownian motion. Here, we consider only the trap stiffness in x-direction (the direction of tube pulling), which can be then used in Eq. S1 to obtain the force.

To record the particle and extract its displacement, we used an EMCCD camera with a pixel size of 154×154 nm^2 for the 100× objective lens used in our experiments. To determine the particle position, between 1000 and 2000 images of the bead were recorded (see Fig. S3) at acquisition speed of 47 frames per seconds. The position of the bead was determined using centroid tracking algorithm[4] written in MATLAB (Mathworks Inc). From the obtained bead trajectory (Fig. S3B) we could then determine the trap stiffness using Eq. S2.

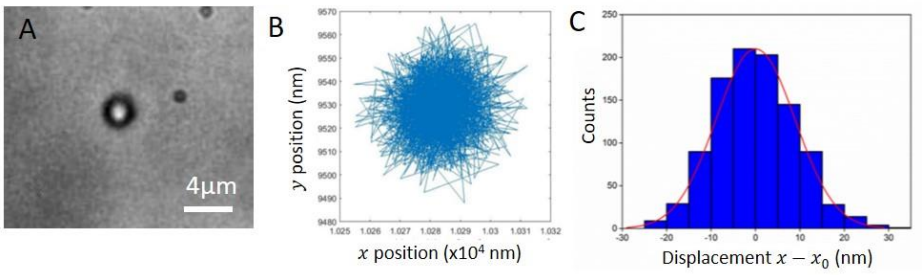

Figure S3. (A) Image of the trapped particle (142×128 pixels), (B) trajectory of the trapped particle recorded from 2000 images, and (C) a histogram of the particle displacement with a Gaussian fit (red curve). Here and in all other measurements, the laser power was set to that used in the tube-pulling experiments.

The camera exposure time and acquisition speed are important parameters affecting the position tracking of the trapped bead. At high exposure times, the position of the bead is averaged by the camera apparently increasing the trap stiffness, while at low exposure times, the noise in the image increases. The apparent trap stiffness measured using the equipartition theorem approach is shown in Fig. S4 for different values of the exposure time. A plateau region with no dependence of the trap stiffness on the exposure time was found for exposure times between 0.67 and 1 ms. Thus, in our experiments, the exposure time was set to be 0.86 ms. This exposure time was also corroborated by agreement between the viscous drag force method and the equipartition theorem approach as shown further.

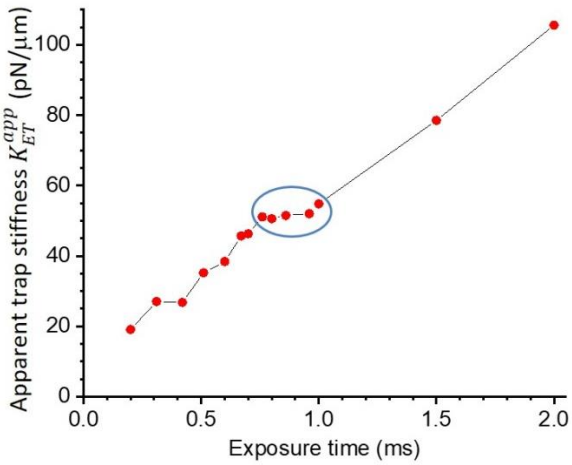

Figure S4. Apparent trap stiffness as a function of the camera exposure time. The data were obtained using the equipartition theorem approach. The plateau region is encircled.

Using the optimized exposure time and acquisition speed, we measured the trap stiffness using different beads (see red data points in Fig. S5). We observed deviations from particle to particle suggesting that the bead size/shape varied, presumably as a result from the streptavidin coating. This implied, that the trap stiffness calibration needs to be performed prior to tube pulling with the very bead used in the measurement.

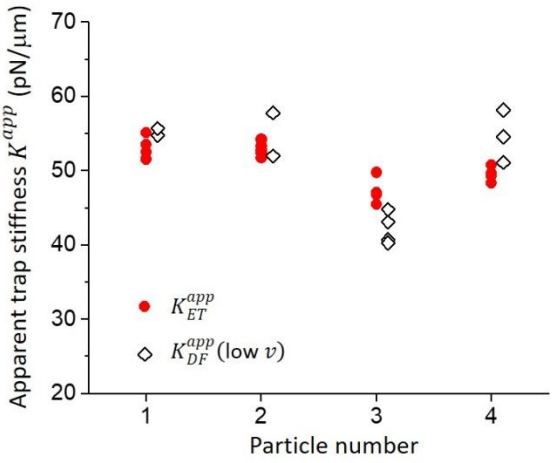

Figure S5. Apparent trap stiffness measured on different particles assessed from the equipartition theorem approach (red circles) and from the drag force at low stage velocity $\boldsymbol{v}$ = 0.5 mm/s (black diamonds), see text for details.

In the experiments when a tube was pulled, the trapped bead gets off-centered, i.e. the bead is located away from the equilibrium point in the focal plane because of the pulled tube. This results in a force different from that when the bead is near the center of the trap (as assessed with the equipartition theorem approach). To estimate the modified trapping force near the edge of the trap, we applied the viscous drag force (DF) method which is based on the application of a hydrodynamic force on the bead. This is implemented by moving the microscope stage. The force is described by the Stokes law:

$$F_{esc} = 6\pi\eta r v_{esc} \quad \text{(S3)}$$

where η is the viscosity of the solution, v_{esc} is the escape velocity (above which the particle leaves the trap) and r is the radius of the bead. The trap stiffness can be then determined from the escape force and the bead off-center displacement at velocity close to v_{esc}:

$$K_{DF} = \frac{F_{esc}}{x - x_0} \tag{S4}$$

It is pertinent to note here that measuring the escape force inside a vesicle suspension often results in losing the particle by collisions with surrounding vesicles as the stage has to be displaced at high velocity. To circumvent these difficulties, we developed the following approach. We measured an apparent trap stiffness (in vesicle free medium) for different stage velocities, v, defined as:

$$K_{DF}^{app}(v) = \frac{6\pi\eta r \Delta v}{\Delta(x - x_0)} \tag{S5}$$

where Δv sets the velocity range. Using Eq. S5, we determined the range of stage velocities, which yields apparent trap stiffness equal to that obtained with the equipartition theorem approach, $K_{ET}^{app} = K_{DF}^{app}(v)$, see Fig. S5. This range included low velocities between 0.2 and 0.8 mm/s.

As indicated above, in the tube-pulling experiments the bead is off-centered relocating to the periphery of the trap potential well because of the pulled tube. This significantly alters the force. We thus introduced a correction factor to account for this difference resulting from the off-centering. This correction factor is the ratio between the apparent trap forces measured at high and low stage velocities, $K_{DF}^{app}(\text{high } v)$ and $K_{DF}^{app}(\text{low } v)$, respectively. The range of high stage velocities corresponds to off-center displacement $x - x_0$ falling in the range of those measured during tube pulling. Figure S6 shows the off-center displacement in the two different velocity ranges. The slopes of the data yields $K_{DF}^{app}(\text{high } v)$ and $K_{DF}^{app}(\text{low } v)$.

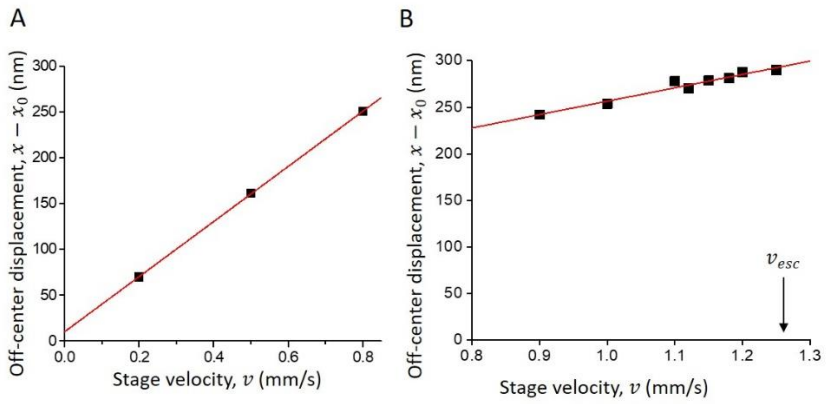

Figure S6. Bead off-center displacement $\boldsymbol{x - x_0}$ for (A) low and (B) high velocity of the stage. The two data sets were collected on the same bead. The slopes of the linear fits were used to determine $\boldsymbol{K_{DF}^{app}}(\text{low } \boldsymbol{v})$ and $\boldsymbol{K_{DF}^{app}}(\text{high } \boldsymbol{v})$, respectively.

Finally, the trap stiffness for each particle inside the vesicle suspension was estimated from measuring the apparent value from the equipartition theorem approach, K_{ET}^{app}, which was then corrected as follows:

$$K = K_{ET}^{app} \frac{K_{DF}^{app}(\text{high } v)}{K_{DF}^{app}(\text{low } v)} \quad \text{(S6)}$$

In our experiments the trap stiffness values were found to vary between 92.52 and 108.16 pN/μm for the different particles.

Section S5. Tube pulling experiment in high NaCl and KCl and vesicle leakage

In high salt concentrations, GUVs were grown in sucrose and then diluted in solutions of high concentrations of NaCl and KCl, separately. In these conditions, GUVs became very sticky to each other and some tubes were observed resulting from vesicle-vesicle adhesion and displacement. This could affect the pulling force if we used such vesicles interconnected with tubes. Besides the long tubes, we observed small outward protrusions which could be due to the adhesion of small vesicles and lipid patches to the GUVs. To work around this problem, we decreased the amount of lipid used to spread lipid on the ITO glasses while making GUVs. This decreased the possibility for vesicles contact. Moreover, in high asymmetry conditions, a few vesicles were found to have leaked as observed from their lower contrast. In this regard, we encapsulated 0.2 mol % of Rhodamine B (Sigma) in the GUVs prior to dilution in high salinity solutions. Figure S7A represents images of a vesicle containing Rhodamine B whereas Fig. S7B shows a vesicle which has lost its asymmetry and is not visible in epifluorescence microscopy. The lack of asymmetry in such vesicles does affect the spontaneous curvature. In this regard, we performed tube pulling experiment on two leaked vesicles and found that the lost asymmetry changes both the bending rigidity and the spontaneous curvature of vesicles to the values comparable to our results obtained at low NaCl asymmetry conditions (Fig. S7C and D). As shown in Fig. S7D, the loss of asymmetry leads to negligible spontaneous curvature, while vesicles with preserved asymmetry (intact) exhibit negative spontaneous curvatures. Similar results were obtained on leaked vesicles prepared with high KCl asymmetry (data not shown).

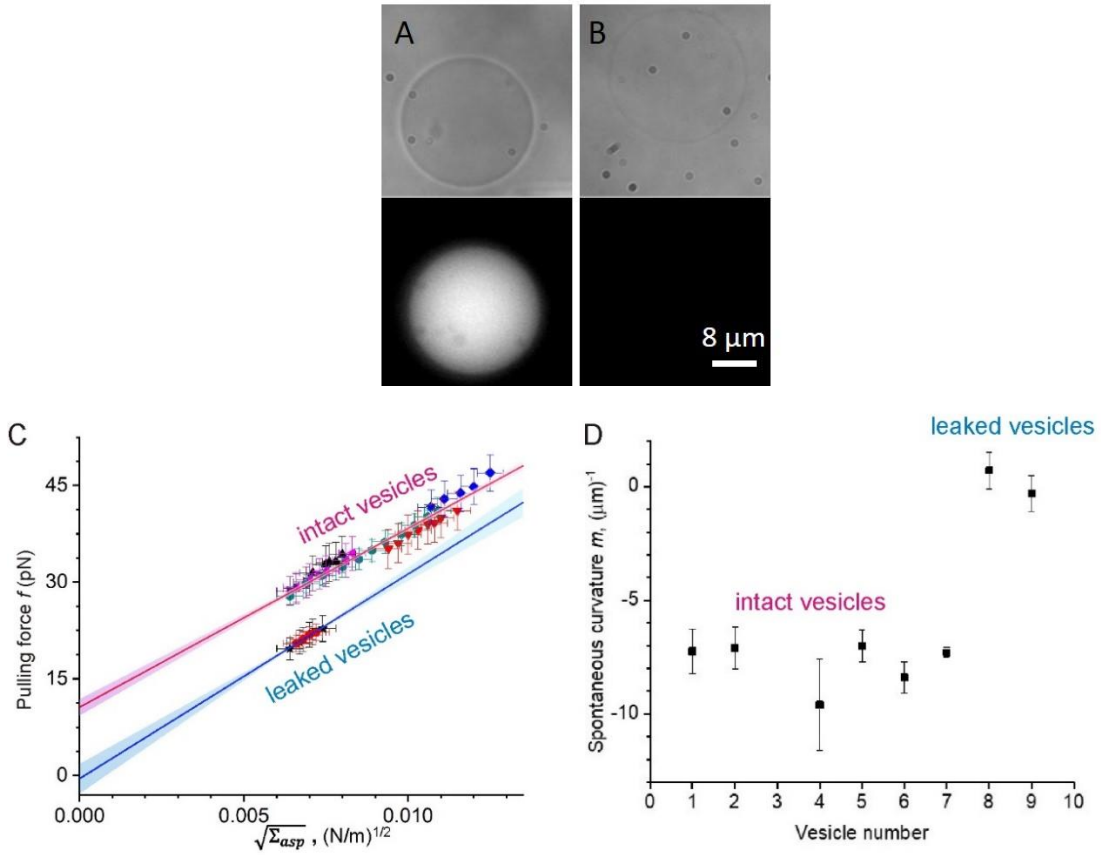

Figure S7. Imaging and measurements on intact and leaked vesicles prepared in the presence of Rhodamine B (encapsulated in their interior) and diluted in higly-concentrated NaCl solution corresponding to in high asymmetry of NaCl. (A, B) Bright field (upper panels) and apiflurescence images (lower panles) of GUVs. In one case, the vesicle has remained intact during the dilution step and is with preserved contrast (A), while in the other case, the vesicle has leaked and lost both contrast in bright field and in epifluorescence (B). (C) Tube pulling experiment on leaked and intact vesicles. (D) Data on the spontaneous curvature values in high NaCl asymmetry for intact and leaked vesicles.

Section S6. Mechanical properties of membrane under different asymmetry of sucrose and salt

The values of the bending rigidity and spontaneous curvature for each individual vesicle at different conditions are summarized in Tables S1-S5:

Table S1. The bending rigidity and spontaneous curvature for each individual vesicle exposed to low asymmetry of sucrose inside and NaCl outside the membrane.

Vesicle number	Bending rigidity (K_BT)	Spontaneous curvature (µm^{-1})
1	31.87±1.70	0.39±0.67
2	31.63±1.94	-0.26±1.10
3	33.57±1.28	0.79±0.50
4	32.84±1.63	-0.04±0.57
5	31.38±1.21	-0.43±0.58
Mean	32.25±1.55	0.09±0.68

Table S2. The bending rigidity and spontaneous curvature for each individual vesicle exposed to high asymmetry of sucrose inside and NaCl outside the membrane.

Vesicle number	Bending rigidity (K_BT)	Spontaneous curvature (μm^{-1})
1	27.49±2.43	-7.23±1.73
2	24.33±1.11	-7.15±1.12
3	23.74±2.16	-9.69±2.55
4	26.76±0.97	-7.03±0.71
5	24.57±3.16	-8.31±2.27
6	25.06±0.46	-7.47±0.38
Mean	25.32±1.71	-7.81±1.46

Table S3. The bending rigidity and spontaneous curvature for each individual vesicle exposed to low asymmetry of sucrose inside and KCl outside the membrane.

Vesicle number	Bending rigidity (K_BT)	Spontaneous curvature (μm^{-1})
1	34.06±0.31	-0.24±0.16
2	34.79±3.64	+0.45±1.70
Mean	34.42±1.9	0.12±1.35

Table S4. The bending rigidity and spontaneous curvature for each individual vesicle exposed to high asymmetry of sucrose inside and KCl outside the membrane.

Vesicle number	Bending rigidity (K_BT)	Spontaneous curvature (μm^{-1})
1	20.19±0.68	-10.64±0.34
2	26.52±1.84	-6.59±1.27
3	25.79±0.34	-6.44±0.26
4	24.57±0.82	-7.28±0.73
Mean	24.08±0.92	-7.73±0.65

Table S5. The bending rigidity and spontaneous curvature for each individual vesicle exposed to low asymmetry of sucrose inside and LiCl outside the membrane.

Vesicle number	Bending rigidity (K_BT)	Spontaneous curvature (μm^{-1})
1	17.37±0.46	-4.67±0.60
2	17.03±1.26	-5.05±1.62
3	18.85±0.77	-3.39±0.99
4	18.90±1.92	-2.73±2.09
Mean	18.03±1.09	-3.94±1.01

Section S7. Fluctuation analysis

The fluctuation analysis is based on collecting a time sequence of snapshots of the thermal fluctuations of the GUVs. Following the detailed description of this technique in [5], we measured the bending rigidity of the POPC vesicles which were exposed to different asymmetry conditions. The vesicle contours were precisely located in phase contrast images recorded using the fast digital camera HG-100K (Redlake Inc., San Diego, CA). Afterwards, the shape fluctuation analysis of the contours was performed to measure the bending rigidity[5]. We recorded a total of 5000 - 10000 snapshots per vesicle with exposure time of 200 μs and typical acquisition speed of 50 frames per second (fps). Only vesicles with clearly visible fluctuations and no visible defects were considered for analysis.

Section S8. Fluorescence lifetime measurements

In an attempt to resolve the nature of interaction of the different ions (suspected condensing effect of lithium ions versus depletion of sodium and potassium ions from the membrane), we performed fluorescence lifetime measurements of the membrane dye DiI. The fluorescence lifetime of this dye was previously shown to depend on the bilayer structure[6]. To this end, the GUVs were immersed in the high or low asymmetry salt buffers and the fluorescence lifetime of POPC GUV doped with 0.2 mol% of DiI was measured (ABBERIOR Instruments, 561 laser in pulsed mode). Fluorescence decays were fitted using SPCImage 5.3. Photon-counts were integrated over one quadrant of an individual GUV. If GUVs exhibited tubes or defects, only the segments of the smooth GUV membrane was considered. Fluorescent decays were fit using two-component exponentials and the weighted mean lifetime was reported. The instrument response function (IRF) was measured using DASPI dye dissolved in methanol. The IRF was then used to deconvolute the measurement data (parameters “shift” and “scatter” were fit using the SPCImage software). The lifetime measured for low and high NaCl and KCl asymmetry (as defined in Table 1 in the main text) were found similar and independent of salt concentration, see Fig. S8, with values close to literature data[6] for egg PC membranes (of which POPC is the major component). This suggests that no significant interaction in terms of intercalation in the membrane is observed for these salts and sugar. On the contrary, the lifetime distribution for the case of low LiCl asymmetry is significantly different ($p<0.05$) compared to the other monovalent salts, suggesting stronger interaction of the lithium ions with the membrane potentially implying intercalation or ion-induced lipid condensation.

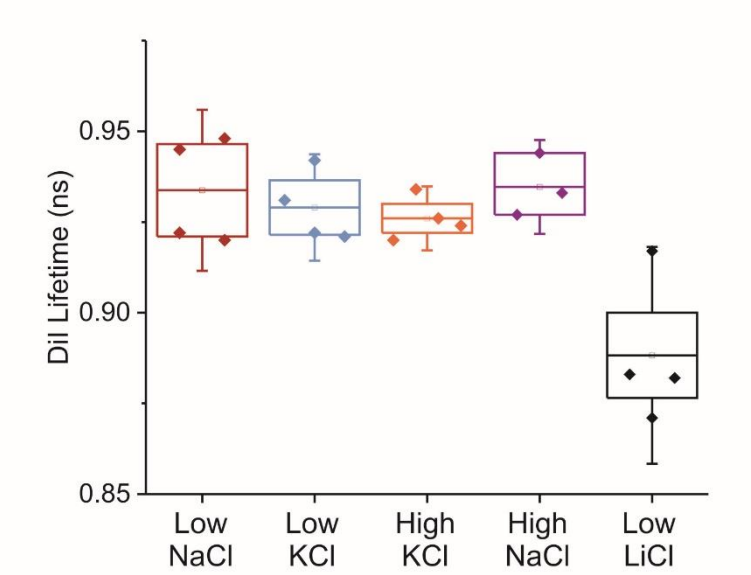

Figure S8. Fluorescence lifetime of DiI dye in the GUV membrane at varying solution asymmetry as defined in Table 1 in the main text.

References

1. Angelova, M. I.; Soléau, S.; Méléard, P.; Faucon, F.; Bothorel, P., Preparation of giant vesicles by external AC electric fields. Kinetics and applications. In *Trends Coll. Interf. Sci.*, Helm, C.; Lösche, M.; Möhwald, H., Eds. Steinkopff: 1992; Vol. 89, pp 127-131.
2. Kraikivski, P.; Pouligny, B.; Dimova, R., Implementing both short- and long-working-distance optical trappings into a commercial microscope. *Rev. Sci. Instrum.* **2006,** *77* (11), 113703.
3. Vitkova, V.; Genova, J.; Bivas, I., Permeability and the hidden area of lipid bilayers. *European Biophysics Journal with Biophysics Letters* **2004,** *33* (8), 706-714.
4. Dasgupta, R.; Verma, R. S.; Gupta, P. K., Microfluidic sorting with blinking optical traps. *Opt. Lett.* **2012,** *37* (10), 1739-1741.
5. Gracià, R. S.; Bezlyepkina, N.; Knorr, R. L.; Lipowsky, R.; Dimova, R., Effect of cholesterol on the rigidity of saturated and unsaturated membranes: fluctuation and electrodeformation analysis of giant vesicles. *Soft Matter* **2010,** *6* (7), 1472-1482.
6. Packard, B. S.; Wolf, D. E., Fluorescence lifetimes of carbocyanine lipid analogs in phospholipid bilayers. *Biochemistry* **1985,** *24* (19), 5176-5181.